Journal of Alloys and Compounds 507 (2010) 120–125

Contents lists available at ScienceDirect

Journal of Alloys and Compounds

journal homepage: www.elsevier.com/locate/jallcom

First-principles study of structural, elastic, electronic and lattice dynamic properties of $As_xP_yN_{1-x-y}Al$ quaternary alloys

B. Ghebouli [a,*], M.A. Ghebouli [b], M. Fatmi [c], T. Chihi [d], S. Boucetta [d]

[a] Laboratoire d'Etudes de Surfaces et Interfaces des Matériaux Solides (LESIMS), Université Ferhat Abbas, Sétif 19000, Algeria
[b] Département de Physique, Centre Universitaire, Bordj-Bou-Arréridj 34000, Algeria
[c] Laboratoire de Physique et Mécanique des Matériaux Métalliques (LP3 M), Université Ferhat Abbas, Sétif 19000, Algeria
[d] Laboratoire d'Elaboration de Nouveaux Matériaux et leurs Caractérisation (ENMC), Université Ferhat Abbas, Sétif 19000, Algeria

ARTICLE INFO

Article history:
Received 7 August 2009
Accepted 14 July 2010
Available online 4 August 2010

Keywords:
Electronic structure
Optical properties
Lattice matched and mismatched alloys
Pseudopotential calculations

ABSTRACT

Information on the energy band gaps, the lattice parameters and the lattice matching to available substrates is a prerequisite for many practical applications. A pseudopotential plane-wave method as implemented in the ABINIT code is used to the $As_xP_yN_{1-x-y}Al$ quaternary alloys lattice matched to AlP substrate to predict their energy band gaps and optical properties. The range of compositions for which the alloy is lattice-matched to AlP is determined. Very good agreement is obtained between the calculated values and the available experimental data. The Debye temperature increase when the bulk modulus is enhanced. We study the variation of elastic constants, the optical phonon frequencies (ω_{TO} and ω_{LO}), the static and high-frequency dielectric coefficient $\varepsilon(0)$ and $\varepsilon(\infty)$ and the dynamic effective charge Z^* with P concentration (y).

1. Introduction

Alloying in the group-V–III has diversified the properties of semiconductor materials, enabling their production with wide band gaps. These semiconductors are used to produce commercially important high-performance electronic and optoelectronic devices and systems, such as light emitting devices covering many regions of the visible spectrum.

The availability of the quaternary alloy $As_xP_yN_{1-x-y}Al$/AlP structure permits an extra degree of freedom by allowing independent control of the band gap, E_g, and the lattice constant, a_0. Tailoring of these compounds could lead to new semiconductor materials with desired band gaps over a continuous broad spectrum of energies [1–9]. These alloys have emerged as interesting materials for device applications because of their energy band structure and lattice parameters. Recently, the use of quaternary AsPNAl alloys has been proposed as a replacement to the AlP. Furthermore, the use of quaternary films enhances the experimental capability for investigating the effects of strain and piezoelectric fields in quantum wells [10].

In order to help understand and control the materials and device properties, we have carried out a theoretical study of the energy band gaps and elastic properties of the quaternary $As_xP_yN_{1-x-y}Al$, lattice matched to AlP substrate. The electronic structure of the quaternary alloy system is calculated using the pseudopotential plane-wave method as implemented in the ABINIT code. Calculations are performed over the entire composition range of x and y. This paper is organized as follows: A brief introduction was given in Section 1. The computational method adopted for the calculations is described in Section 2. We present our results and compare them to the available experimental data and others previously published theoretical results in Section 3. Then, our work is summarized in Section 4.

2. Computational method

The calculations were performed within the GGA to the DFT, using the pseudopotential plane-wave method as implemented in the ABINIT code [11]. ABINIT computer code is a common project of the Université Catholique of Louvain, Corning Incorporated, and other contributors. Only the outermost electrons of each atom were explicitly considered in the calculation. The effect of the inner electrons and the nucleus (the frozen core) was described within a pseudopotential scheme. We used the Hartwigzen–Goedecker–Hutter scheme [12] to generate the norm-conserving nonlocal pseudopotentials, which results in highly transferable and optimally smooth pseudopotentials. A plane-wave basis set was used to solve the Kohn–Sham equations in the pseudopotential implementation of the DFT–GGA. The Brillouin zone integrations were replaced by discrete summations over a

* Corresponding author. Tel.: +213 790629751; fax: +213 35 63 05 60.
E-mail address: bghebouli@yahoo.fr (B. Ghebouli).

0925-8388/$ – see front matter © 2010 Elsevier B.V. All rights reserved.
doi:10.1016/j.jallcom.2010.07.111

special set of k-points, using the standard k-point technique of Monkhorst and Pack [13] where the k-point mesh used is $(8 \times 8 \times 8)$. The plane-wave energy cutoff to expand the wave functions is set to be 90 Hartree (1 Hartree = 27.211396 eV). For the treatment of the disordered ternary alloy, we used the VCA [14], in which the alloy pseudopotentials are constructed within a first-principles VCA scheme. Elemental ionic pseudopotentials of AsAl and AlPN are combined to construct the virtual pseudopotential of $As_xP_yN_{1-x-y}Al$. Recently, Marques et al. [15] have reported a linear behavior of the lattice parameter of $Al_xGa_yIn_{1-x-y}N$ as a function of the composition x, y. Thus, the Vegard's rule has been assumed for the calculation of the lattice constant of quaternary alloys under study [16].

$$a_{VCA} = xa_{AsAl} + ya_{PAl} + (1 - x - y)a_{AlN} \quad (1)$$

3. Results

3.1. Structural properties

The equilibrium lattice parameter is computed from the structural optimization, using the Broyden–Fletcher–Goldfarb–Shanno minimization [17–20]. The lattice matching conditions for $As_xP_yN_{1-x-y}Al$ quaternary systems on the AlP substrate is: $y = 1 - 1.196x$ (Fig. 1). The results of lattice parameter a_0 for different composition rates (x, y) are reported in Table 1. Fig. 2 shows the lattice parameter plotted versus P concentration (y). The deviation from the linear dependence is distinct. An analytical relation for the compositional dependence of $As_xP_yN_{1-x-y}Al$ lattice parameter is given by quadratic fit:

$$a = 5.6381 - 0.125y - 0.012y^2 \quad (2)$$

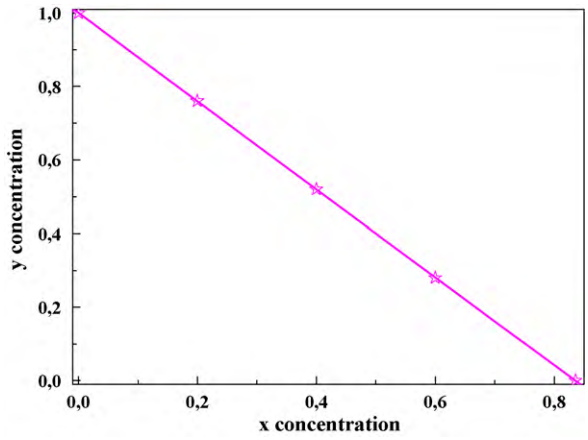

Fig. 1. Lattice matching conditions for $As_xP_yN_{1-x-y}Al$ quaternary systems on the AlP substrate.

3.2. Elastic properties

The elastic constants are important parameters that describe the response to an applied macroscopic stress. In Table 1, the calculated elastic constants (C_{11}, C_{12} and C_{44}), bulk modulus B, shear modulus G, shear wave modulus C_s, Young's modulus E, Kleinman parameter ζ and Poisson's ratio, υ of $As_xP_yN_{1-x-y}Al$ compounds at zero pressure and for various compositions (y) in the range (0–1) are presented. Also given for comparison are the available experimental data and other works for AlP. To the best of our knowledge, no experimental data have been reported so far for the elastic constants of $As_xP_yN_{1-x-y}Al$ in the $0 < y < 1$ composition range. In

Table 1
The calculated lattice constant a_0, bulk modulus B, elastic constants C_{11}, C_{12} and C_{44}, shear modulus G, shear wave modulus C_s, Young's modulus E, Kleinman parameter ζ and Poisson's ratio, υ of $As_xP_yN_{1-x-y}Al$ compounds at zero pressure.

Parameters	References	$x=0$ $y=1$	$x=0.2$ $y=0.76$	$x=0.4$ $y=0.52$	$x=0.6$ $y=0.28$	$x=0.836$ $y=0$
a_0 (Å)	This work	5.5	5.536	5.569	5.601	5.638
	Experiment	[a]5.4672				
	Other works	[b]5.48				
C_{11} (GPa)	This work	122.23	119.13	115.21	111.24	106.84
	Other works	[c]132.25				
C_{12} (GPa)	This work	62.67	60.38	57.85	55.49	52.96
	Other works	[d]61.2, [a]63				
C_{44} (GPa)	This work	57.63	57	55.63	54.16	52.35
	Other works	[b]61.5				
B (GPa)	This work	82.52	79.96	76.97	74.07	70.92
	Experiment	[f]86				
	Other works	[e]82.46				
C_s	This work	29.78	29.37	28.68	27.87	26.94
	Other works	[a]32.9				
ζ	This work	0.635	0.627	0.626	0.624	0.621
	Other works	[e]0.631				
G	This work	44.21	43.68	42.64	41.48	40.09
	Other works	[e]59				
E	This work	112.54	110.86	107.98	104.88	101.21
	Other works	[e]145.6				
υ	This work	0.27	0.2989	0.2661	0.264	0.2621
	Other works	[e]0.2314				

[a] [28].
[b] [29].
[c] [30].
[d] [31].
[e] [32].
[f] [33].

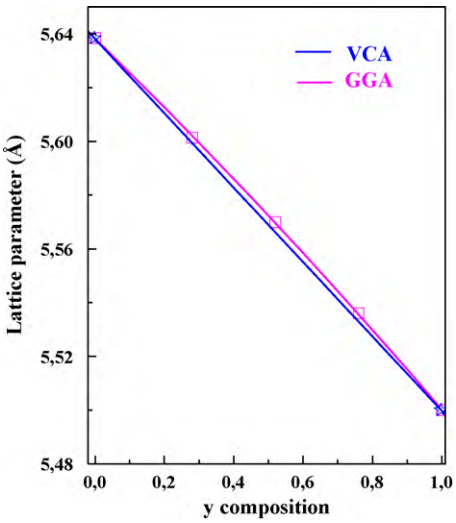

Fig. 2. Relaxed lattice parameter of $As_xP_yN_{1-x-y}Al/AlP$ structure as a function of P composition (y).

Fig. 3, we depict the composition dependence of the elastic constants (C_{11}, C_{12} and C_{44}) of $As_xP_yN_{1-x-y}Al$. We observe a linear dependence in all curves in the considered range of composition. It is easy to observe that the elastic constants C_{ij} increase monotonously when the composition (y) is enhanced. From the theoretical elastic constants, we computed the elastic wave velocities. The single-crystal elastic wave velocities in different directions are given by the resolution of the Cristoffel equation [21]:

$$(C_{ijkl} \cdot n_j \cdot n_k - \rho v^2 \cdot \delta_{il})u_l = 0 \tag{3}$$

where C_{ijkl} is the single-crystal elastic constant tensor, n is the propagation direction, ρ is the density of material, u is the wave polarization and v is the wave velocity. The solutions of this equation are of two types: a longitudinal-wave with polarization parallel to the direction of propagation v_l and two shear waves v_{T1} and v_{T2} with polarization perpendicular to n. Another important parameter is the elastic anisotropy factor, A, which gives a measure of the anisotropy of the elastic wave velocity in a crystal. In a cubic crystal, the elastic anisotropy factor is given by [22]:

$$A = \frac{2C_{44} + C_{12}}{C_{11}} - 1 \tag{4}$$

which is zero for an isotropic material. The variation of the longitudinal-wave mode speed (V_L) and transverse-wave mode speed (V_T) in $As_xP_yN_{1-x-y}Al/AlP$ structure propagating in the [1 0 0], [1 1 0] and [1 1 1] directions at zero pressure for various P composition (y) in the range (0–1) are shown in Fig. 4. It seen that, longitudinal-waves are fastest along [1 1 1] and shear waves are slowest along [1 1 0] for $As_xP_yN_{1-x-y}Al/AlP$ structure which has a positive elastic anisotropy factor. The curves presented are the best fit of the calculated data. The analytical expressions of V_L and V_T are as follows:

$$\begin{aligned}
V_L^{100}(\mathrm{m/s}) &= 5326.289 + 902.015y + 892.573y^2 \\
V_T^{100}(\mathrm{m/s}) &= 3727.22 + 651.375y + 522.067y^2 \\
V_L^{111}(\mathrm{m/s}) &= 6112.33 + 1030.381y + 989.004y^2 \\
V_T^{111}(\mathrm{m/s}) &= 3065.698 + 506.454y + 454.268y^2 \\
V_L^{110}(\mathrm{m/s}) &= 5925.597 + 999.98y + 965.568y^2 \\
V_{T1}^{110}(\mathrm{m/s}) &= 2674.077 + 441.158y + 400.097y^2 \\
V_{T2}^{110}(\mathrm{m/s}) &= 3727.495 + 616.677y + 546.76y^2
\end{aligned} \tag{5}$$

One can note that longitudinal-wave mode speed and transverse-wave mode speed increase monotonously with increasing P composition (y) in the range (0–1).

Once the elastic constants are determined, we would like to compare our results with experiments, or predict what experiment would yield for the elastic constants. For cubic crystal, the isotropic bulk modulus B and the shear constant C_s are given exactly by:

$$B = \frac{C_{11} + 2C_{12}}{3} \quad \text{and} \quad C_s = \frac{1}{2}(C_{11} - C_{12}) \tag{6}$$

Another important parameter is the Kleinman parameter, ζ, which describes the relative positions of the cation and anion sublattices under volume-conserving strain distortions for which positions are not fixed by symmetry. It is known that a low value of ζ implies there is a large resistance against bond bending or bond-angle distortion and vice versa [23,24]. We calculated the ζ value using the following relation [25]:

$$\zeta = \frac{C_{11} + 8C_{12}}{7C_{11} + 2C_{12}} \tag{7}$$

We also calculated Young's modulus E and Poisson's ratio ν which are frequently measured for polycrystalline materials when investigating their hardness. These quantities are related to the bulk modulus and the shear modulus by the following equations [26]:

$$\begin{aligned}
E &= \frac{9BG}{3B + G} \\
\nu &= \frac{3B - E}{6B}
\end{aligned} \tag{8}$$

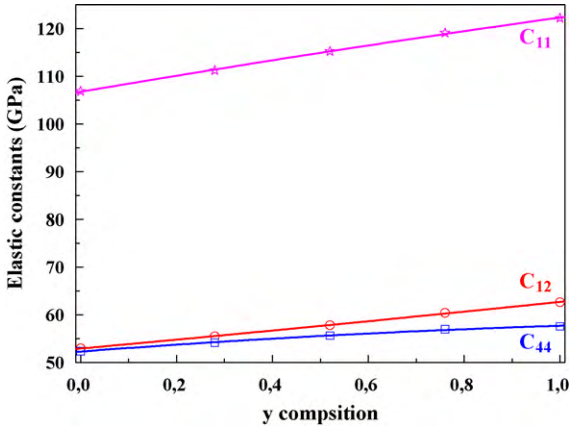

Fig. 3. Composition dependence of the elastic constants in $As_xP_yN_{1-x-y}Al/AlP$ structure.

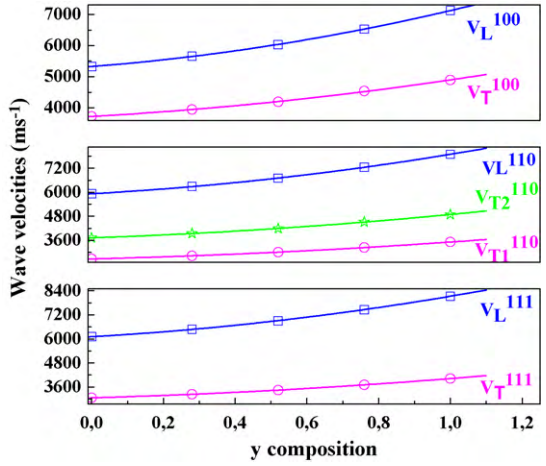

Fig. 4. The longitudinal-wave mode speed (V_L) and transverse-wave mode speed (V_T) in $As_xP_yN_{1-x-y}Al/AlP$ structure propagating in the [1 0 0], [1 1 0] and [1 1 1] directions at zero pressure for various y composition.

Table 2
The calculated density ρ, the longitudinal, transverse and average sound velocity v_l, v_t and v_m calculated from polycrystalline elastic modulus, and Debye temperatures θ_D calculated from the average sound velocity of $As_xP_yN_{1-x-y}Al$ compounds at zero pressure.

References	ρ (g cm^{-3})	v_l (ms^{-1})	v_t (ms^{-1})	v_m (ms^{-1})	θ_D (K)
AlP	2.40986	7662.09	4283.42	4768.3	431.71
$As_{0.2}P_{0.76}N_{0.04}Al$	2.79672	7029.82	3952.209	4397.586	418.41
$As_{0.4}P_{0.52}N_{0.08}Al$	3.16466	6502.87	3670.72	4038.027	404.82
$As_{0.6}P_{0.28}N_{0.12}Al$	3.48029	6097.36	3452.61	3839.42	392.93
$As_{0.836}N_{0.164}Al$	3.76841	5745.17	3261.97	3626.61	381.11

3.3. Calculation of Debye temperature

Having calculated Young's modulus E, bulk modulus B and shear modulus G, one can calculate the Debye temperature, which is an important fundamental parameter closely related to many physical properties such as elastic constants, specific heat and melting temperature. At low temperature, the vibrational excitations arise solely from acoustic mode. Hence, at low temperature the Debye temperature calculated from elastic constants is the same as that determined from specific heat measurements. One of the standard methods to calculate the Debye temperature θ_D is from elastic data, since θ_D may be estimated from the average sound velocity v_m by the following equation [27]:

$$\theta_D = \frac{h}{k_B}\left(\frac{3n}{4\pi V_a}\right)^{1/3} v_m \quad (9)$$

where h is the Plank's constant, k_B is the Boltzmann's constant and V_a is the atomic volume. The average sound velocity in the polycrystalline material is given by [21]:

$$v_m = \left[\frac{1}{3}\left(\frac{2}{v_1^2} + \frac{1}{v_t^3}\right)\right]^{-1/3} \quad (10)$$

where v_l and v_t are the longitudinal and transverse sound velocity of an isotropic aggregate obtained using the shear modulus G and the bulk modulus B from Navier's equation [26]:

$$v_1 = \left(\frac{3B+4G}{3\rho}\right)^{1/2} \quad \text{and} \quad v_t = \left(\frac{G}{\rho}\right)^{1/2} \quad (11)$$

The calculated sound velocities and Debye temperature as well as the density of $As_xP_yN_{1-x-y}Al$/AlP structure are given in Table 2. The Dependence of Debye temperature and bulk modulus with P composition (y) for $As_xP_yN_{1-x-y}Al$/AlP structure are shown in Fig. 5. One can note that Debye temperature and bulk modulus increase with increasing P composition (y). The Debye temperature increase when the bulk modulus is enhanced.

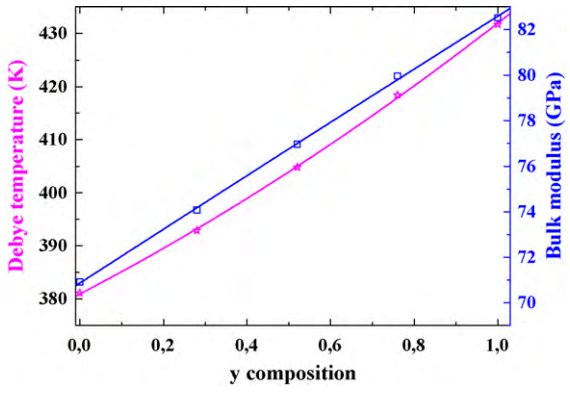

Fig. 5. Dependence of Debye temperature and bulk modulus with y composition for $As_xP_yN_{1-x-y}$ Al/AlP structure.

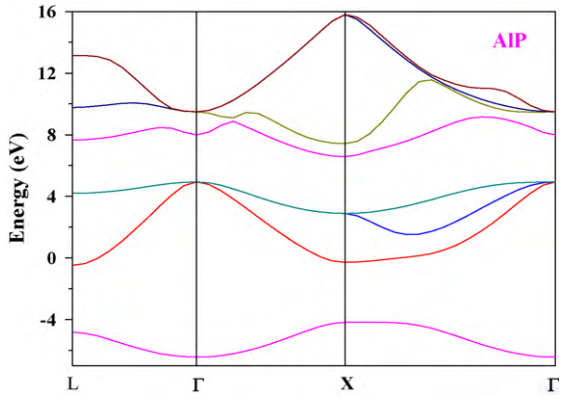

Fig. 6. Band structure of AlP substrate.

3.4. Electronic properties

The band structure of $As_xP_yN_{1-x-y}Al$ lattice matched to AlP was calculated through the high-symmetry points Γ, X and L in the Brillouin zone. These compounds show that there is an indirect band gaps because of the bottom of the conduction band and the top of the valence band are found to be at Γ and X respectively. The band structure of AlP substrate is shown in Fig. 6. Direct band gaps ($\Gamma-\Gamma$), ($L-L$) and ($X-X$) and indirect band gaps ($\Gamma-L$) and ($\Gamma-X$) of $As_xP_yN_{1-x-y}Al$ at zero pressure are shown in Table 3. The P composition energy variations of the conduction band edges at Γ, X and L with respect to the top of the valence band are obtained. Results are plotted in Fig. 7, which show the dependence of direct and indirect band gap energies, in the lattice matched $As_xP_yN_{1-x-y}Al$/AlP structure, on the P concentration (y). Note that both direct and indirect band gaps namely ($\Gamma-\Gamma$), ($L-L$) and ($\Gamma-L$) increase monotonically with increasing the (y) composition. This is not the case for the direct and indirect band-gap ($X-X$) and ($\Gamma-X$) which change non-monotonically. In order to provide analytical expressions for the energy band gaps of the $As_xP_yN_{1-x-y}Al$ quaternary system which could be of practical use and of easy access, we obtained the following analytical expressions by fitting

Table 3
Some direct band gaps ($\Gamma-\Gamma$, $L-L$, $X-X$) and indirect band gaps ($\Gamma-L$, $\Gamma-X$) of $As_xP_yN_{1-x-y}Al$ at zero pressure.

Elements	$\Gamma-\Gamma$ (eV)	$L-L$ (eV)	$X-X$ (eV)	$\Gamma-L$ (eV)	$\Gamma-X$ (eV)
AlP					
This work	3.049	3.463	3.688	2.714	1.63
Experiment	[c]3.63				[b]2.45
Others	[a]3.073				[a]1.635
$As_{0.2}P_{0.76}N_{0.04}Al$	2.719	3.358	3.708	2.591	1.628
$As_{0.4}P_{0.52}N_{0.08}Al$	2.409	3.242	3.704	2.466	1.615
$As_{0.6}P_{0.28}N_{0.12}Al$	2.107	2.335	3.688	2.335	1.593
$As_{0.836}N_{0.164}Al$	1.767	2.176	3.658	2.176	1.559

[a] [34].
[b] [35].
[c] [36].

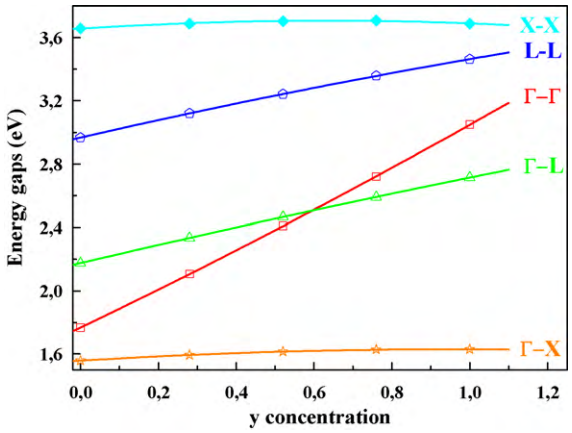

Fig. 7. Direct ($\Gamma-\Gamma$), ($L-L$) and ($X-X$) and indirect ($\Gamma-L$) and ($\Gamma-X$) band-gap energies in $As_xP_yN_{1-x-y}Al/AlP$ quaternary alloys as a function of y concentration.

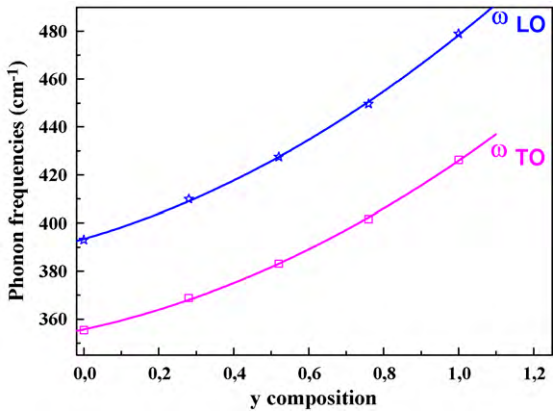

Fig. 8. Frequencies of the longitudinal optical (LO) and transversal optical (TO) phonons in $As_xP_yN_{1-x-y}Al/AlP$ quaternary alloys as function of y concentration.

our energy gaps data using a least squares procedure:

$$\begin{aligned} E_{\Gamma}^{\Gamma} &= 1.768 + 1.178y + 0.101y^2 \\ E_{\Gamma}^{X} &= 1.558 + 0.148y - 0.076y^2 \\ E_{\Gamma}^{L} &= 2.175 + 0.576y - 0.038y^2 \\ E_{L}^{L} &= 2.967 + 0.566y - 0.069y^2 \\ E_{X}^{X} &= 3.656 + 0.155y - 0.122y^2 \end{aligned} \quad (12)$$

3.5. Lattice dynamic properties

The numerically longitudinal and transversal optical phonon frequencies, referred to as ω_{LO} and ω_{TO}, respectively of $As_xP_yN_{1-x-y}Al/AlP$ at various compositions (y) are listed in Table 4. Also shown for comparison are the existing experimental and theoretical data in the literature. The agreement between our results and experiment as regards ω_{LO} and ω_{TO} of AlP are better than 4.4% and 2.9%. No comparison has been made in the $0<y<1$ composition range, as there are no known data available to date to the best of our knowledge. The variation of the frequencies of the $_{LO}$ and $_{TO}$ phonons in $As_xP_yN_{1-x-y}Al/AlP$ quaternary alloys as a function of the P concentration (y) are plotted in Fig. 8, one obtains for ω_{LO} and ω_{TO},

$$\begin{aligned} \omega_{LO} &= 393.41 + 44.54y + 40.39y^2 \\ \omega_{TO} &= 355.66 + 33.83y + 36.39y^2 \end{aligned} \quad (13)$$

These expressions may be used to predict the LO and TO phonon frequencies for any P concentration (y) in the range (0–1) for $As_xP_yN_{1-x-y}Al/AlP$ structure. Note also that both ω_{LO} and ω_{TO} change non-linearly and increase as the composition (y) is enhanced. For the same concentration (y), ω_{LO} is greater than ω_{TO}.

A good knowledge of the full electronic structure is an essential feature in order to get the best understanding of the optical properties of semiconductors. Thus, the refractive index which is essential in the design of heterostructure lasers, in optoelectronic devices as well as in solar cell applications has been estimated according to the relation: $\varepsilon(\infty)=n^2$. The knowledge of the dielectric constants makes it possible to proceed with the calculations of the refractive index. The static and high-frequency dielectric constants $\varepsilon(0)$ and $\varepsilon(\infty)$ have been calculated at various P concentrations (y), for the lattice matched $As_xP_yN_{1-x-y}Al/AlP$ structure. Our results are depicted in Table 4. For the fact that both experimental and theoretical data regarding n, $\varepsilon(\infty)$, and $\varepsilon(0)$ for $As_xP_yN_{1-x-y}Al$ lattice matched to AlP were not available, our results are predictions and may serve for reference. The variations of both static and high-frequency dielectric constants as a function of P composition (y) are plotted in Fig. 9. The high-frequency dielectric and static dielectric constants decrease monotonously with increasing P concentration (y). In order to provide analytical expressions for both $\varepsilon(\infty)$ and $\varepsilon(0)$ of the material of interest, the data obtained by our calculations were found to fit best by a least squares procedure giving the following relations:

$$\begin{aligned} \varepsilon(0) &= 12.229 - 1.799y + 0.596y^2 \\ \varepsilon(\infty) &= 9.998 - 1.84y + 0.584y^2 \end{aligned} \quad (14)$$

These expressions may be useful for obtaining $\varepsilon(\infty)$ and $\varepsilon(0)$ for any (y) concentration in $As_xP_yN_{1-x-y}Al$ alloy lattice matched to AlP.

In Fig. 10, the absolute values of the calculated Born effective charge Z^* are plotted as a function of the P concentration y. The value of Z^* increases monotonously with increasing P concentration (y). A quadratic fit to our data gives:

$$Z^* = 2.213 + 0.042y - 0.002y^2 \quad (15)$$

Table 4
Transverse effective charge, the longitudinal optical (LO) and transverse optical (TO) phonon frequencies, The static and high-frequency dielectric constants and refractive index of $As_xP_yN_{1-x-y}Al$ for different y concentration.

Material	Z^*	ω_{LO} (cm^{-1})	ω_{TO} (cm^{-1})	n	$\varepsilon(0)$	$\varepsilon(\infty)$
AlP						
This work	2.2535	478.84	426.3	2.956	11.027	8.7402
Experiment	–	[c]501	[c]439.4		[b]9.8	[a]7.5
Others	[d]2.2	[d]494.9	[d]442.6			[d]8.4
$As_{0.2}P_{0.76}N_{0.04}Al$	2.2443	401.62	449.64	2.99	11.2067	8.9416
$As_{0.4}P_{0.52}N_{0.08}Al$	2.235	383.07	427.48	3.033	11.4556	9.1992
$As_{0.6}P_{0.28}N_{0.12}Al$	2.225	368.74	409.94	3.086	11.772	9.5246
$As_{0.836}N_{0.164}Al$	2.214	355.33	393.01	3.162	12.23	10

[a] [37].
[b] [36].
[c] [38].
[d] [39].

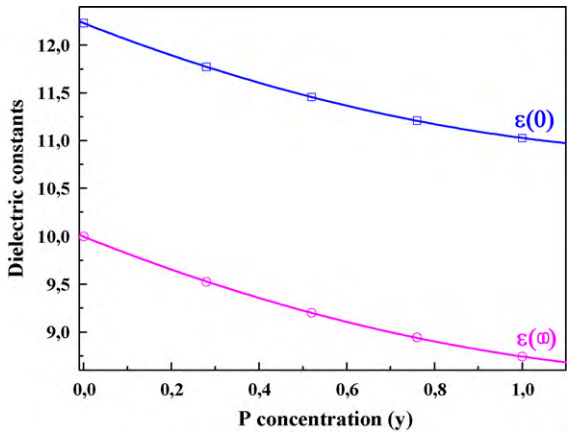

Fig. 9. Static and high-frequency dielectric constants as a function of y concentration for the lattice matched $As_xP_yN_{1-x-y}$Al/A1P structure.

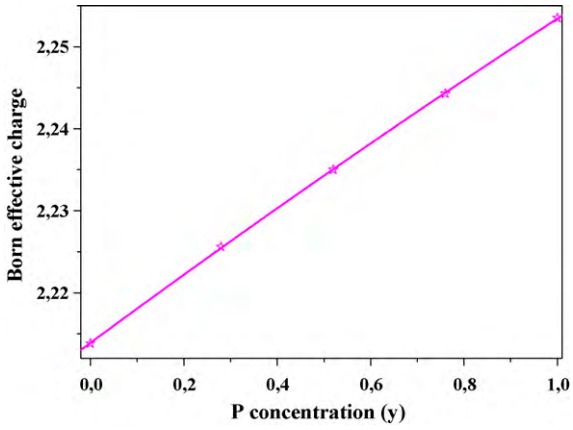

Fig. 10. Dependence of the dynamic effective charge with y composition for $As_xP_yN_{1-x-y}$Al/AlP structure. Solid line is quadratic fit to our data.

4. Conclusion

In conclusion, we studied the composition dependence of energy band gaps and dielectric constants of $As_xP_yN_{1-x-y}$Al quaternary alloys, lattice matched to AlP substrate, by means of the pseudopotential plane-wave method as implemented in the ABINIT code. Based on the calculated lattice constants, we predicted the range of compositions for which AsPNAl is lattice matched to AlP. Very good agreement was obtained between the band gap predictions and available experimental data. Our findings indicate that the high-frequency and the static dielectric constants decrease monotonically with increasing P concentration (y) from 0 to 1. The expressions derived for static and high-frequency dielectric constants as a function of P concentrations are useful for tailoring electric and opto-electric devices based on cubic $As_xP_yN_{1-x-y}$Al quaternary alloys. Due to the lack of experimental and theoretical data regarding the refractive index, high-frequency and static dielectric constants, our results are predictions and may serve as reference for future experimental work.

Acknowledgment

This work is supported by the ENMC and LESIMS Laboratories, University of Setif.

References

[1] J.W. Orton, C.T. Foxon, Rep. Prog. Phys. 61 (1998) 1, and references therein.
[2] S.C. Jain, M. Willander, J. Narayan, R. Van Overstraelen, J. Appl. Phys. 87 (2000) 965, and references therein.
[3] K. Kassali, N. Bouarissa, Microelectron. Eng. 54 (2000) 277.
[4] I. Vurgaftman, J.R. Meyer, J. Appl. Phys. 94 (2003) 3675, and references therein.
[5] S. Nakamura, G. Fasol, The Blue Laser Diode, Springer, Berlin, 1997.
[6] S. Nakamura, Semiconduct. Sci. Technol. 14 (1999) R27.
[7] P. Kung, M. Razegui, Opt. Rev. 8 (2000) 201.
[8] M. Asif Khan, J.N. Kusnia, D.T. Olson, W.J. Schaff, J.W. Burm, M.S. Shur, Appl. Phys. Lett. 65 (1994) 1121.
[9] C.I.H. Ashby, C.C. Willan, J. Han, N.A. Missert, P.P. Provencio, D.M. Follstaedt, G.M. Peake, L. Griego, Appl. Phys. Lett. 77 (2000) 3233.
[10] F.G. McIntosh, K.S. Boutros, J.C. Roberts, S.M. Bedair, E.L. Piner, N.A. El-Masry, Appl. Phys. Lett. 68 (1996) 40.
[11] The ABINIT computer code is a common project of the Universite Catholique de Louvain, Corning Incorporated and Other Contributors. Available online at: http://www.abinit.org.
[12] C. Hartwigsen, S. Goedecker, J. Hutter, Phys. Rev. B 58 (1998) 3641.
[13] H.J. Monkhorst, J.D. Pack, Phys. Rev. B 13 (1976) 5189.
[14] L. Nordheim, Ann. Phys. (Leipzig) 9 (1931) 607.
[15] M. Marques, L.K. Teles, L.M.R. Scolfaro, J.R. Leite, J. Furthmuller, F. Bechstedt, Appl. Phys. Lett. 83 (2003) 890.
[16] A. Hafaiedh, N. Bouarissa, Mater. Chem. Phys. (2009) 122.
[17] C.G. Broyden, J. Inst. Math. Appl. 6 (1970) 222.
[18] R. Fletcher, Comput. J. 13 (1970) 317.
[19] D. Goldfarb, Math. Comput. 24 (1970) 23.
[20] D.F. Shanno, Math. Comput. 24 (1970) 647.
[21] O.L. Anderson, J. Phys. Chem. Solids 24 (1963) 909.
[22] S.E. Lofland, J.D. Hettinger, A. Bryan, P. Finkel, S. Gupta, M.W. Barsoum, G. Hug, Phys. Rev. B 74 (2006) 174501.
[23] K. Kim, W.R.L. Lambrecht, B. Segal, Phys. Rev. B 50 (1994) 1502.
[24] L. Kleinman, Phys. Rev. B 12 (1962) 2614.
[25] W.A. Harrison, Electronic Structure and Properties of Solids, Dover, New York, 1989.
[26] M.W. Barsoum, T. El-Raghi, W.D. Porter, H. Wang, S. Chakraborty, J. Appl. Phys. 88 (2000) 6313.
[27] P. Wachter, M. Filzmoser, J. Rebisant, J. Phys. B 293 (2001) 199.
[28] I. Vurgaftman, J.R. Meyer, L.R. Ram-Mohan, J. Appl. Phys. 89 (2001) 5815.
[29] Landolt-Börstein, Semicondutors: Physics of Group IV Elements and III–V Compounds, vol. III/17a, Springer-Verlag, Berlin, 1992.
[30] M.J. Herrera-Cabrera, P. Rodriguez-Hernandez, A. Munoz, Phys. Stat. Sol. (b) 223 (2001) 411.
[31] T. Azuhata, T. Sota, K. Suzuki, J. Phys. Condens. Matter 8 (1996) 3111.
[32] A. Bouhemadou, R. Khenata, M. Kharoubi, T. Seddik, H. Ali, Y. Reshak, Al. Douri, Comput. Mater. Sci. 45 (2009) 474.
[33] M.L. Cohen, Phys. Rev. B 32 (1985) 7988.
[34] L.H. Yu, et al., Solid State Commun. 135 (2005) 124.
[35] M.R. Lorenz, R. Chikotka, G.D. Pettit, P.J. Dean, Solid State Commun. 8 (1970) 693.
[36] B. Monemar, Phys. Rev. B (1973) 5711.
[37] A. Dal Corso, F. Mauri, A. Rubio, Phys. Rev. B (1996) 15638.
[38] A. Onton, Proc. 10th Int. Conf. Physics of Semiconductors, Cambridge, Mass, 1970, USAC, Oak Ridge, 1970.
[39] S. Aouadi, P. Rodriguez-Hernandez, K. Kassali, A. Muñoz, Phys. Lett. A 372 (2008) 5340.